

Supplementary Materials

UNRAVELING AIE IN ZINC(II) COORDINATION COMPLEXES: ROLE OF LIGAND STRUCTURE AND MECHANISTIC INSIGHTS

Y. Oleksii,^a Y. Cheret,^a M. Allain,^a A. Brosseau,^a S. Haacke,^b A. El-Ghayoury^{*a}

^a Univ Angers, CNRS, MOLTECH – Anjou, SFR MATRIX, F-49000 Angers, France

^b Institut de Physique et Chimie des Matériaux de Strasbourg (IPCMS) UMR 7504, CNRS,
Université de Strasbourg, 23 rue du Loess, Strasbourg 67083, France

* Corresponding author: abdelkrim.elghayoury@univ-angers.fr

CONTENTS

Table S1. Crystal data and structure refinement for ZnL¹	4
Fig. S1. Crystal packing diagram showing the arrangement of ZnL¹ complexes with counter ions and solvent molecules along the <i>b</i> -axis.....	5
Fig. S2. Hydrogen bonding interactions between the hydroxyl (-OH) group of a methanol solvent molecule and a neighboring perchlorate counter-ion within the crystal structure of ZnL¹ , as highlighted by dashed lines (see Table S2 for details).	5
Table S2. Hydrogen bonds parameters (Å, °) for ZnL¹	6
Table S3. Crystal data and structure refinement for ZnL²	6
Fig. S3. Absorption (a) and Emission ($\lambda_{\text{exc}} = 315 \text{ nm}$) (b) spectra of $1.0 \times 10^{-5} \text{ mol} \cdot \text{L}^{-1}$ L¹ in the mixed solvent of water and THF system with different f_w	7
Fig. S4. Absorption (a) and Emission ($\lambda_{\text{exc}} = 314 \text{ nm}$) (b) spectra of $1.0 \times 10^{-5} \text{ mol} \cdot \text{L}^{-1}$ ZnL¹ in the mixed solvent of water and MeCN system with different f_w	7
Fig. S5. Absorption (a) and Emission ($\lambda_{\text{exc}} = 341 \text{ nm}$) (b) spectra of $1.0 \times 10^{-5} \text{ mol} \cdot \text{L}^{-1}$ L² in the mixed solvent of water and THF system with different f_w	7
Fig. S6. Corresponding changes in fluorescence peak intensities of ZnL² (I/I_0 , I_0 = fluorescence intensity in MeCN solution) in different f_w	8
Fig. S7. 2D trace recorded for L² for time range 1 ns. Data recorded for THF sample at concentration of 10^{-5} M at room temperature.....	8
Fig. S8. Kinetic trace obtained of L² for time range 1 ns. Data recorded for THF sample at concentration of 10^{-5} M at room temperature ($\tau = 0,03299 \text{ ns}$).....	9
Fig. S9. Kinetic traces obtained of ZnL² with 0%, 80% and 90% of water percentage	9
Note S1. Relationship Between Fluorescence Lifetime and Steady-State Fluorescence intensity	10
Fig. S10. Infrared spectra of L¹	12
Fig. S11. Infrared spectra of ZnL¹	12
Fig. S12. Infrared spectra of L²	13
Fig. S13. Infrared spectra of ZnL²	13
Fig. S14. ^1H NMR (300 MHz, Chloroform- <i>d</i>) L¹	14
Fig. S15. ^{13}C NMR (126 MHz, Chloroform- <i>d</i>) L¹	14
Fig. S16. ^1H NMR (300 MHz, Acetonitrile- <i>d</i> ₃) ZnL¹	15
Fig. S17. ^{13}C NMR (126 MHz, Acetonitrile- <i>d</i> ₃) ZnL¹	15
Fig. S18. ^1H NMR (300 MHz, Chloroform- <i>d</i>) L²	16
Fig. S19. ^{13}C NMR (126 MHz, Chloroform- <i>d</i>) L²	16
Fig. S20. ^1H NMR (300 MHz, Acetonitrile- <i>d</i> ₃) ZnL²	17
Fig. S21. ^{13}C NMR ((126 MHz, Acetonitrile- <i>d</i> ₃) ZnL²	17
Fig. S22. ESI-MS: L¹	18

Fig. S23. ESI-MS: ZnL¹	18
Fig. S24. HR-MS: L²	19
Fig. S25. ESI-MS: ZnL²	19

Table S1. Crystal data and structure refinement for **ZnL¹**.

Empirical formula	C ₄₀ H ₃₄ Cl ₂ N ₁₀ O ₁₀ S ₂ Zn
Formula weight, g/mol	1015.16
Temperature, K	200.00(10)
Crystal system	Monoclinic
Space group	I2/a
a/Å	18.4902(11)
b/Å	8.0542(3)
c/Å	28.4759(12)
α/°	90
β/°	90.379(5)
γ/°	90
Cell volume, Å ³	4240.6(3)
Z	4
ρ _{calc} , g/cm ³	1.590
μ, mm ⁻¹	3.499
F(000)	2080
Crystal size, mm ³	0.222 x 0.139 x 0.049
Radiation	Cu Kα ($\lambda = 1.54184$) 2Θ range for data collection 6.208° to 145.506°
Index ranges	-21 ≤ h ≤ 22, -9 ≤ k ≤ 9, -34 ≤ l ≤ 34
Reflections collected	4284
Independent reflections	4284
Data/restraints/parameters	4284/5/304
Goodness-of-fit on F ²	1.014
Final R indexes [I>=2σ(I)]	R ₁ = 0.0425, wR ₂ = 0.1144
Final R indexes [all data]	R ₁ = 0.0451, wR ₂ = 0.1162

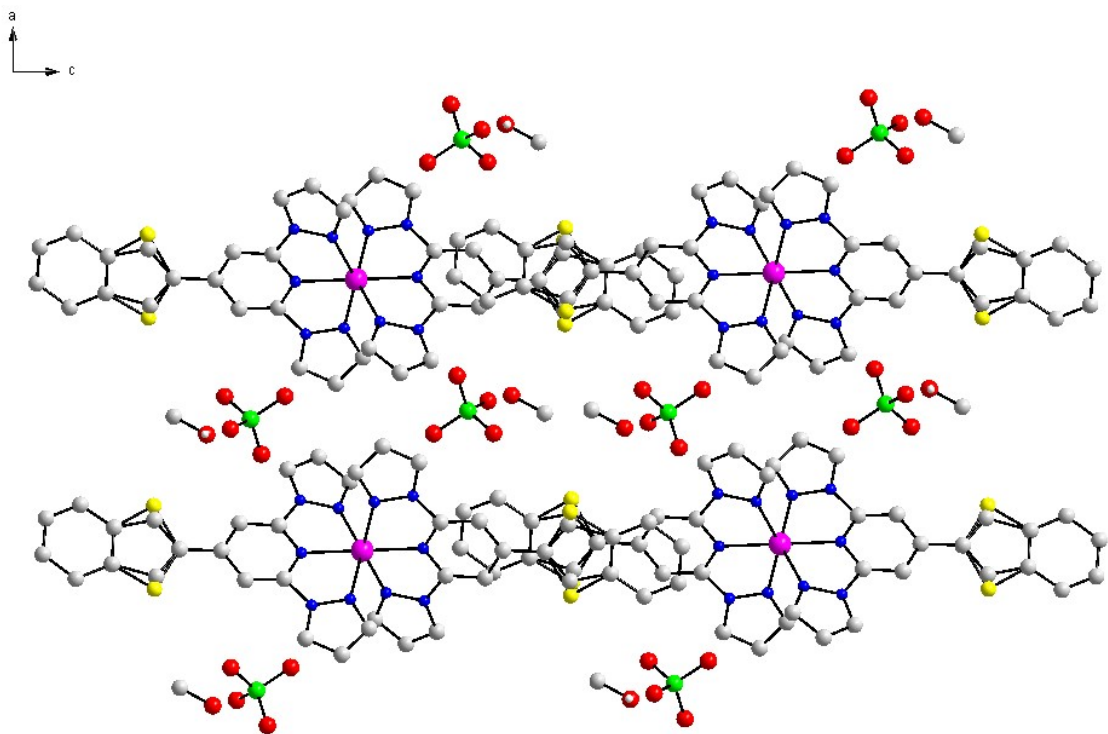


Fig. S1. Crystal packing diagram showing the arrangement of **ZnL¹** complexes with counter ions and solvent molecules along the *b*-axis

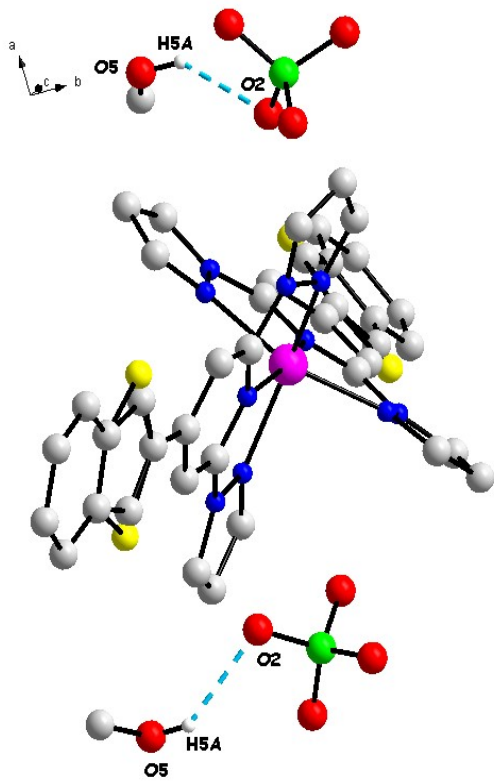


Fig. S2. Hydrogen bonding interactions between the hydroxyl (-OH) group of a methanol solvent molecule and a neighboring perchlorate counter-ion within the crystal structure of **ZnL¹**, as highlighted by dashed lines (see Table S2 for details).

Table S2. Hydrogen bonds parameters (\AA , $^\circ$) for **ZnL¹**.

D-H \cdots A	d (H \cdots A), \AA	d(D \cdots A), \AA	\angle (D-H \cdots A), $^\circ$
O(5)-H(5A) \cdots O(2)	2.217	2.911	139.90

Table S3. Crystal data and structure refinement for **ZnL²**.

Empirical formula	C ₄₄ H ₃₆ Cl ₄ N ₁₀ O ₉ S ₂ Zn
Formula weight, g/mol	1120.12
Temperature, K	200.00(10)
Crystal system	triclinic
Space group	P-1
a/ \AA	13.3088(3)
b/ \AA	14.6201(3)
c/ \AA	14.6236(3)
$\alpha/^\circ$	71.154(2)
$\beta/^\circ$	76.115(2)
$\gamma/^\circ$	64.496(2)
Cell volume, \AA^3	2413.44(10)
Z	2
$\rho_{\text{calc}}, \text{g/cm}^3$	1.541
μ, mm^{-1}	4.113
F(000)	1144
Crystal size, mm ³	0.383 \times 0.168 \times 0.119
Radiation	Cu K α ($\lambda = 1.54184$) 2 Θ range for data collection 6.432° to 152.296°
Index ranges	-15 \leq h \leq 14, -18 \leq k \leq 18, -18 \leq l \leq 18
Reflections collected	44155
Independent reflections	9750 [$R_{\text{int}} = 0.0398$, $R_{\text{sigma}} = 0.0223$]
Data/restraints/parameters	9750/135/669
Goodness-of-fit on F ²	1.038
Final R indexes [I \geq =2 σ (I)]	$R_1 = 0.0466$, $wR_2 = 0.1296$
Final R indexes [all data]	$R_1 = 0.0491$, $wR_2 = 0.1325$

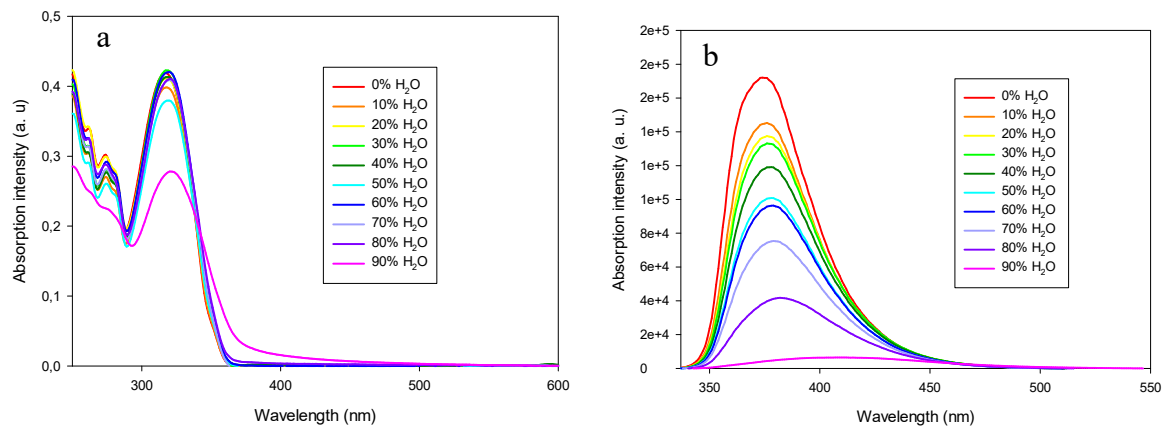


Fig. S3. Absorption (a) and Emission ($\lambda_{\text{exc}} = 315 \text{ nm}$) (b) spectra of $1.0 \times 10^{-5} \text{ mol} \cdot \text{L}^{-1}$ \mathbf{L}^1 in the mixed solvent of water and THF system with different f_w

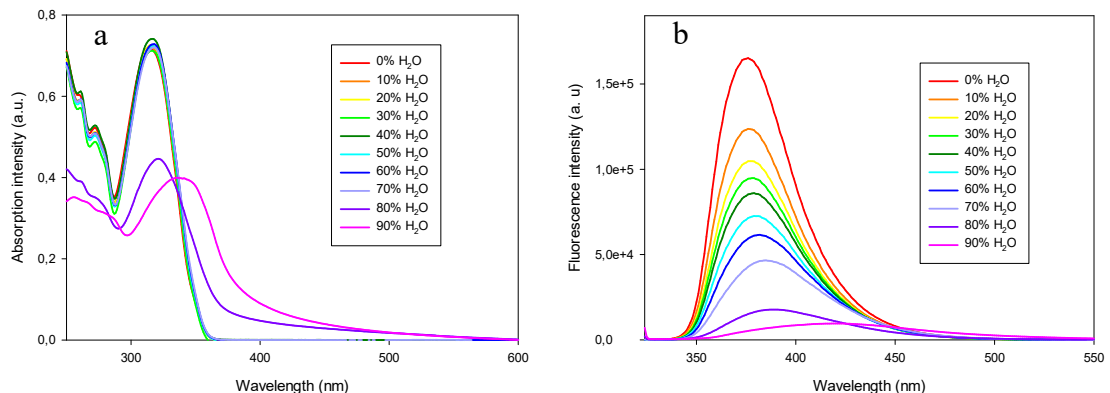


Fig. S4. Absorption (a) and Emission ($\lambda_{\text{exc}} = 314 \text{ nm}$) (b) spectra of $1.0 \times 10^{-5} \text{ mol} \cdot \text{L}^{-1}$ \mathbf{ZnL}^1 in the mixed solvent of water and MeCN system with different f_w

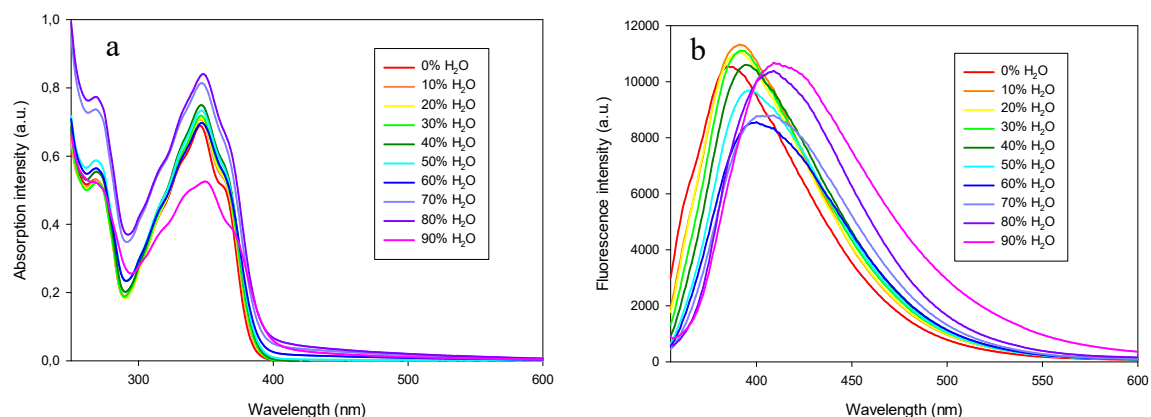


Fig. S5. Absorption (a) and Emission ($\lambda_{\text{exc}} = 341 \text{ nm}$) (b) spectra of $1.0 \times 10^{-5} \text{ mol} \cdot \text{L}^{-1}$ \mathbf{L}^2 in the mixed solvent of water and THF system with different f_w

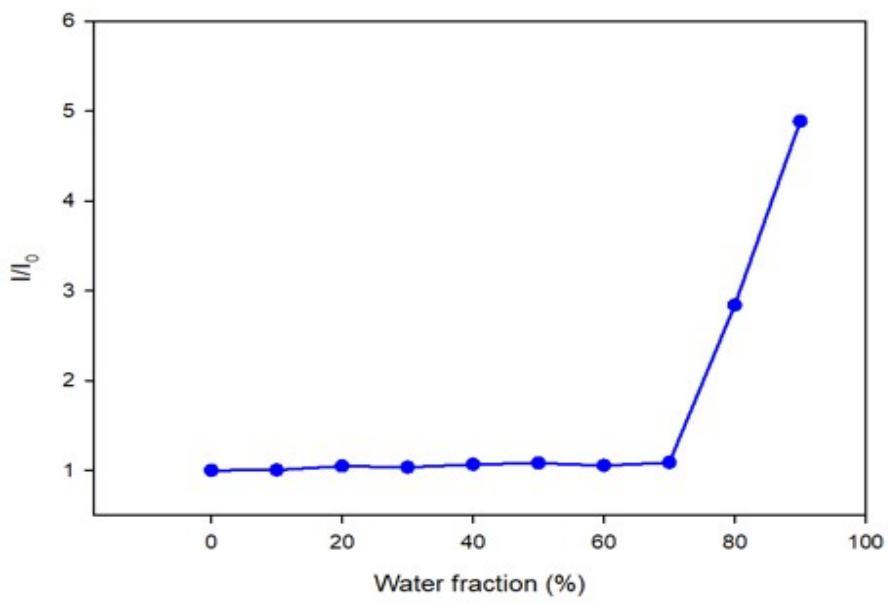


Fig.S6. Corresponding changes in fluorescence peak intensities of \mathbf{ZnL}^2 (I/I_0 , I_0 = fluorescence intensity in MeCN solution) in different f_w

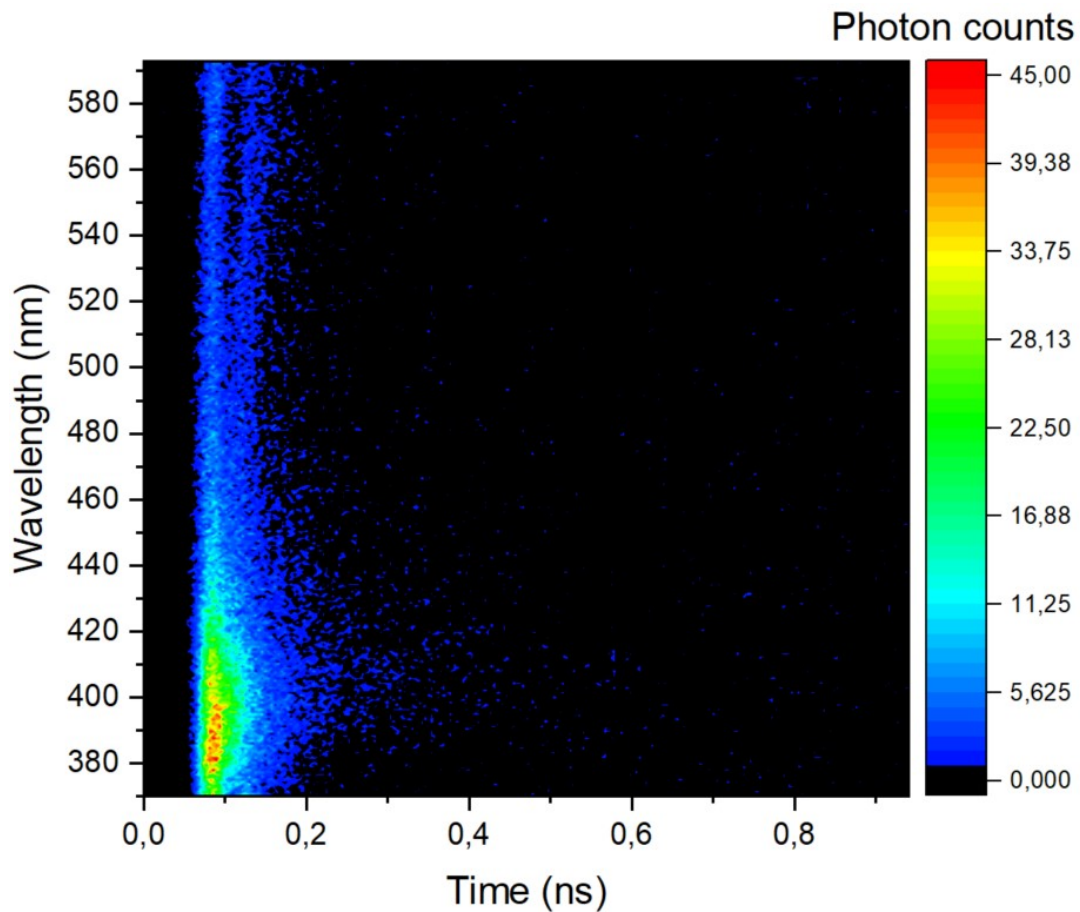


Fig. S7. 2D trace recorded for \mathbf{L}^2 for time range 1 ns. Data recorded for THF sample at concentration of 10^{-5} M at room temperature

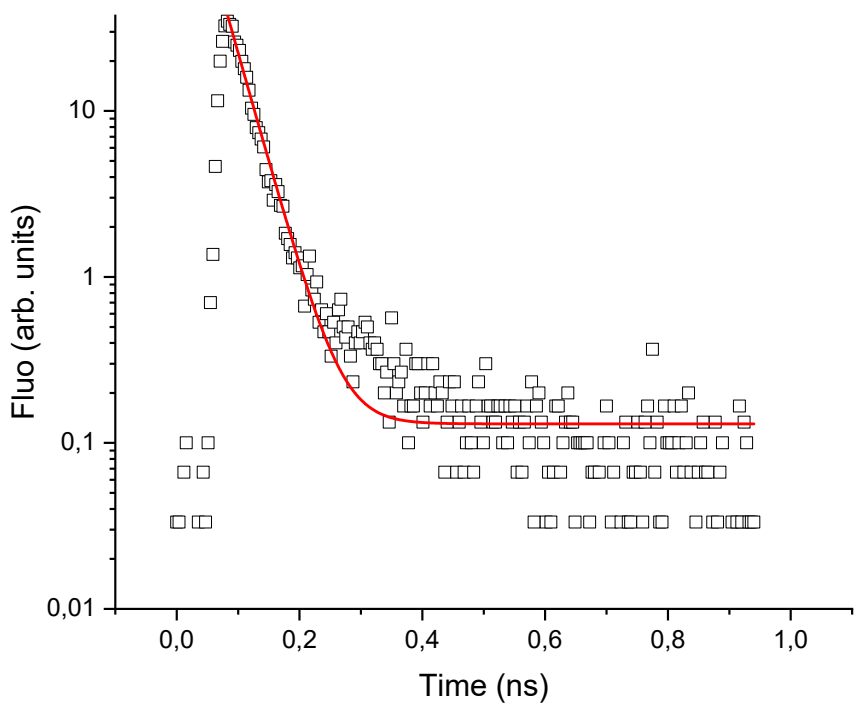


Fig. S8. Kinetic trace obtained of L^2 for time range 1 ns. Data recorded for THF sample at concentration of 10^{-5} M at room temperature ($\tau = 0,03299$ ns)

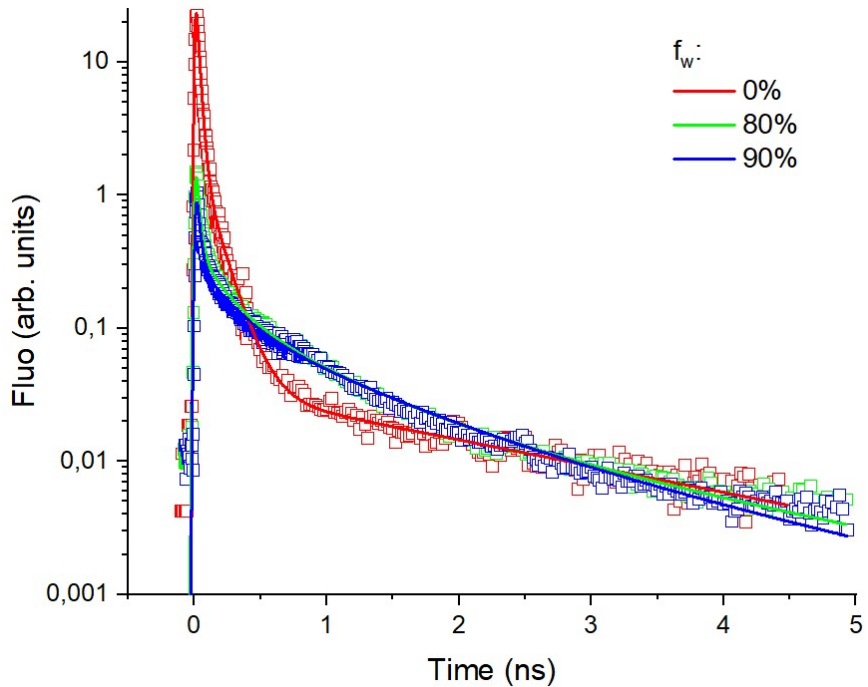


Fig. S9. Kinetic traces obtained of ZnL^2 with 0%, 80% and 90% of water percentage

Note S1. Relationship Between Fluorescence Lifetime and Steady-State Fluorescence intensity

In fluorescence studies involving molecular aggregation, the relationship between the amplitude-weighted average lifetime $\langle \tau \rangle$ and the time-integrated fluorescence signal is essential for interpreting the origin of emission enhancement. Here, we provide a mathematical and conceptual justification for comparing steady-state fluorescence intensities with time-resolved fluorescence lifetimes, especially in systems where spectrally distinct emissive species cannot be resolved.

In this derivation, we show that the steady-state fluorescence intensity is proportional to the amplitude-weighted average fluorescence lifetime $\langle \tau \rangle$, under the assumption that absorption at the excitation wavelength remains approximately constant across samples.

The fluorescence QY is defined as:

$$\Phi_f = \frac{\text{Number of emitted photons}}{\text{Number of absorbed photons}}$$

Experimentally, it is determined by measuring the temporally and spectrally integrated fluorescence signal $\int_{\lambda em} F^u(\lambda) d\lambda$ with respect to the one of a reference sample, with a known Φ_f , and normalising with respect to the different amount of absorption at the excitation wavelength $f_r(\lambda_{ex})$:

$$\Phi_f^u = \Phi_f^r \frac{f_r(\lambda_{ex})}{f_u(\lambda_{ex})} \cdot \frac{\int_{\lambda em} F^u(\lambda) d\lambda}{\int_{\lambda em} F^r(\lambda) d\lambda} \cdot \frac{n_u^2}{n_r^2}$$

Here, u and r denote the “unknown” and “reference” samples, respectively. Since the solvents are the same, the ratio of refractive indices n_u and n_r is 1. This approach is used to relate the steady-state fluorescence intensities to the time-resolved fluorescence lifetimes. The absorption at the excitation wavelength λ_{ex} is related to the absorbance A by:

$$f(\cdot)(\lambda_{ex}) = 1 - 10^{-A(\cdot)(\lambda_{ex})}$$

When comparing the Φ_f of the two samples with different water fractions (x and y), the ratio simplifies to:

$$\frac{\Phi_f^y}{\Phi_f^x} = \frac{f_x(\lambda_{ex})}{f_y(\lambda_{ex})} \cdot \frac{\int_{\lambda em} F^y(\lambda) d\lambda}{\int_{\lambda em} F^x(\lambda) d\lambda}$$

where the integral are carried out over the full emission spectral range. How does the temporally integrated fluorescence signal $\int_{\lambda em} F^u(\lambda) d\lambda$ relate to the time-resolved kinetics? It is proportional to the time integral of the fluorescence decay:

$$\int_{em} F^u(\lambda) d\lambda = C \int_0^\infty I_0 \left(\sum_{i=1}^N A_i e^{-t/\tau_i} \right) dt$$

Where, C is a proportionality factor describing the sensitivity of the instrument, and I_0 is the intensity signal at $t=0$, which is proportional to the excitation power, the absorption $f(\lambda_{ex})$, and the radiative rate of the fluorophore. The temporal integral goes over the sum of

$$\sum_{i=1}^N A_i \tau_i \int_0^\infty A_i e^{-t/\tau_i} dt = A_i \tau_i$$

exponentials and is simply given by $\sum_{i=1}^N A_i \tau_i$, since $\int_0^\infty A_i e^{-t/\tau_i} dt = A_i \tau_i$. When we now relate the ratio of the time-integrated fluorescence signals to the temporal integral of kinetics we find:

$$\frac{\int_{em} F^y(\lambda) d\lambda}{\int_{em} F^x(\lambda) d\lambda} = \frac{\left[\int_0^\infty I_0 \left(\sum_{i=1}^N A_i e^{-t/\tau_i} \right) dt \right]_y}{\left[\int_0^\infty I_0 \left(\sum_{i=1}^N A_i e^{-t/\tau_i} \right) dt \right]_x} = \frac{I_0^y}{I_0^x} \cdot \frac{\left[\sum_{i=1}^N A_i \tau_i \right]_y}{\left[\sum_{i=1}^N A_i \tau_i \right]_x}$$

$$<\tau_y> = \left[\sum_{i=1}^N A_i \tau_i \right]_y \quad \text{and}$$

The average lifetimes calculated in the paper are

$$<\tau_x> = \left[\sum_{i=1}^N A_i \tau_i \right]_y \quad \text{since } \sum_{i=1}^N A_i = 1$$

. Hence, we have :

$$\frac{\int_{em} F^y(\lambda) d\lambda}{\int_{em} F^x(\lambda) d\lambda} = \frac{I_0^y}{I_0^x} \cdot \frac{<\tau_y>}{<\tau_x>}$$

Now, back to the ratio of the Φ_f 's:

$$\frac{\Phi_f^y}{\Phi_f^x} = \frac{f_x(\lambda_{ex})}{f_y(\lambda_{ex})} \cdot \frac{\int_{em} F^y(\lambda) d\lambda}{\int_{em} F^x(\lambda) d\lambda} = \frac{f_x(\lambda_{ex})}{f_y(\lambda_{ex})} \cdot \frac{I_0^y}{I_0^x} \cdot \frac{<\tau_y>}{<\tau_x>}$$

Finally, since I_0 scales with absorption and excitation power (which are the same for both samples), we can simplify:

$$\frac{\Phi_f^y}{\Phi_f^x} = \frac{\int_{em} F^y(\lambda) d\lambda}{\int_{em} F^x(\lambda) d\lambda} = \frac{<\tau_y>}{<\tau_x>}$$

In our system, AIE is observed with increasing water content in MeCN. However, the emission spectra of weakly emissive monomeric species and their aggregated counterparts overlap significantly. Therefore, spectral separation is not feasible, and both time-resolved and spectrally integrated steady-state data must be considered together to evaluate emission behavior.

The observed proportionality between $<\tau>$ and the steady-state fluorescence intensity across different water fractions (Table 4, Fig. 9b) confirms this theoretical framework. Minor

deviations from perfect proportionality can be attributed to slight variations in absorbance at 341 nm upon aggregation. Nevertheless, the correlation strongly supports that increased emission arises from a reduction of non-radiative decay pathways and stabilization of emissive states due to aggregation.

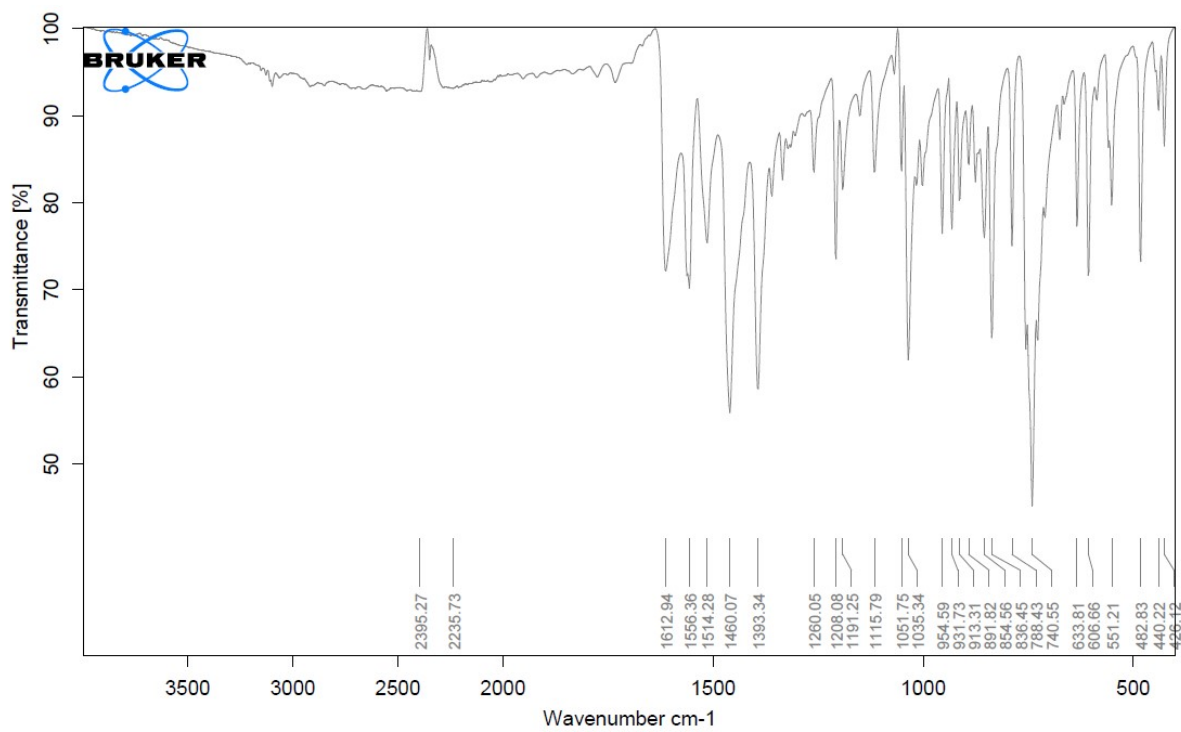


Fig. S10. Infrared spectra of \mathbf{L}^1

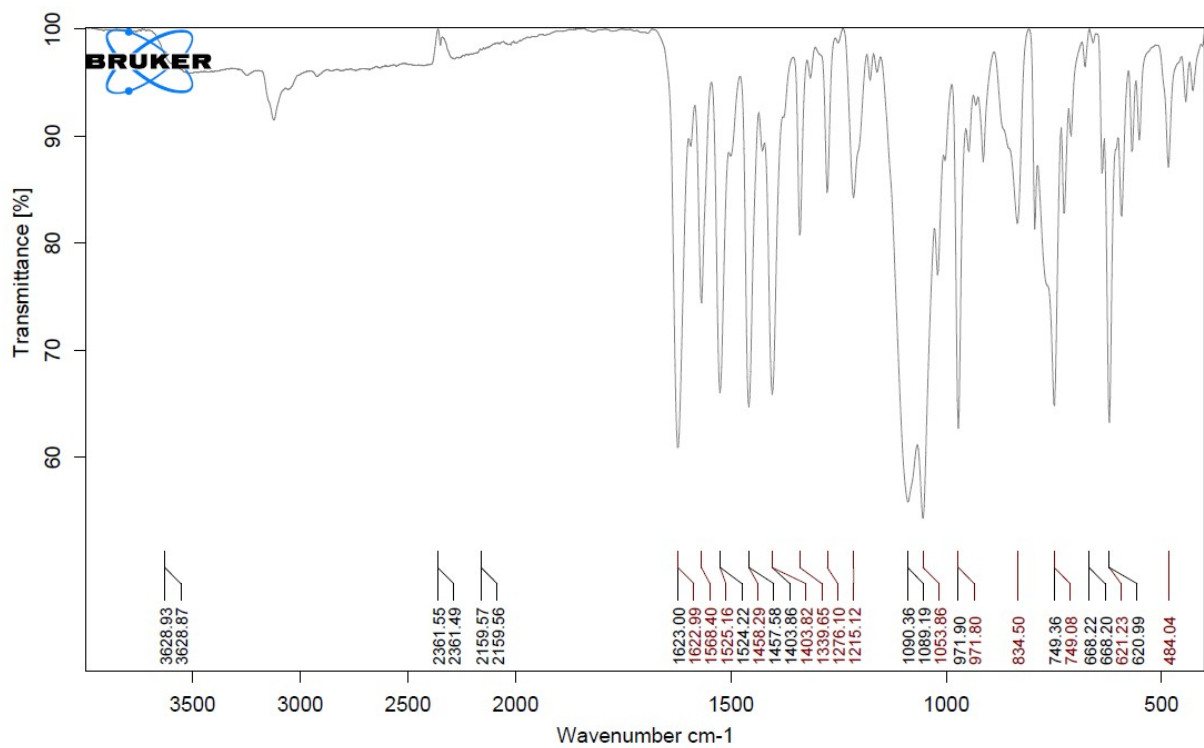


Fig. S11. Infrared spectra of \mathbf{ZnL}^1

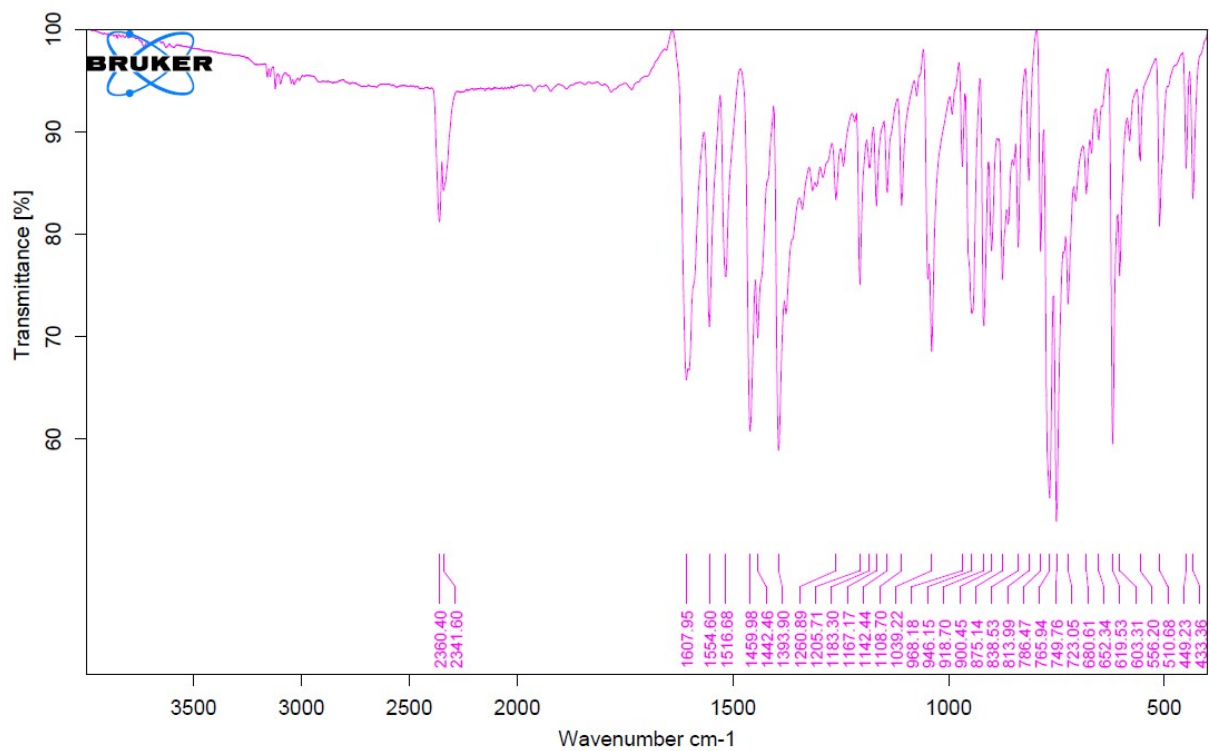


Fig. S12. Infrared spectra of \mathbf{L}^2

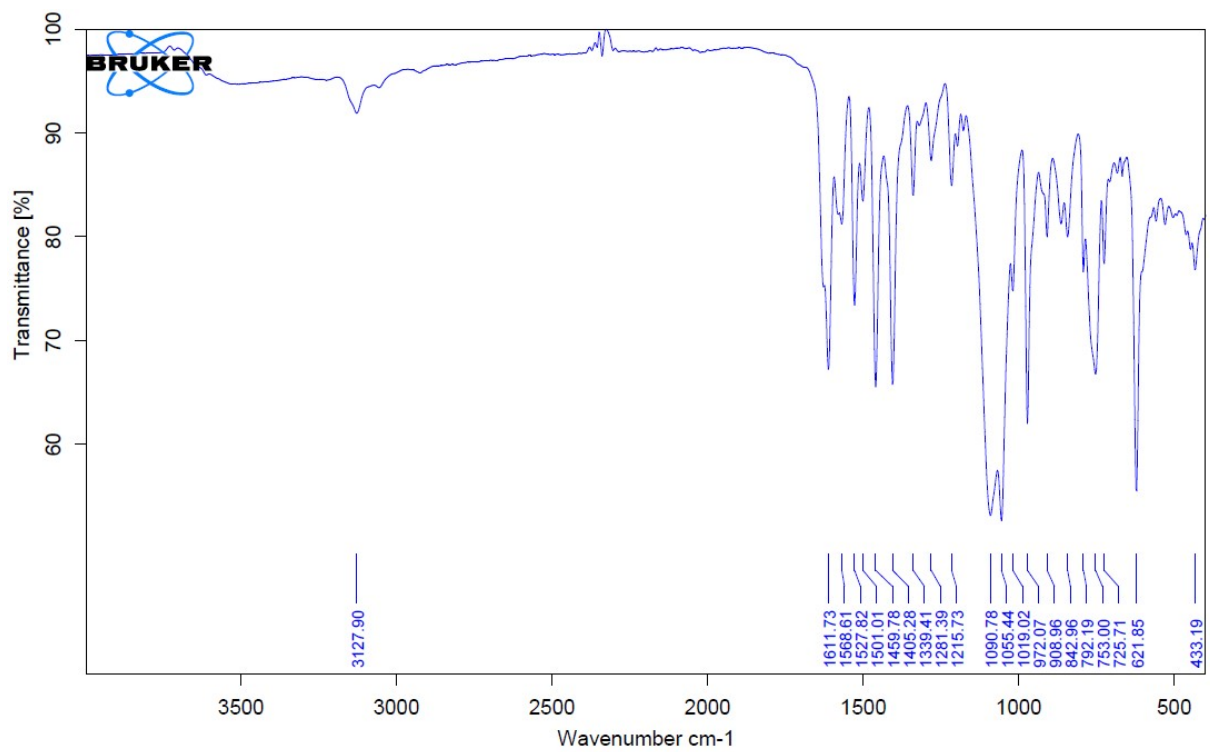


Fig. S13. Infrared spectra of \mathbf{ZnL}^2

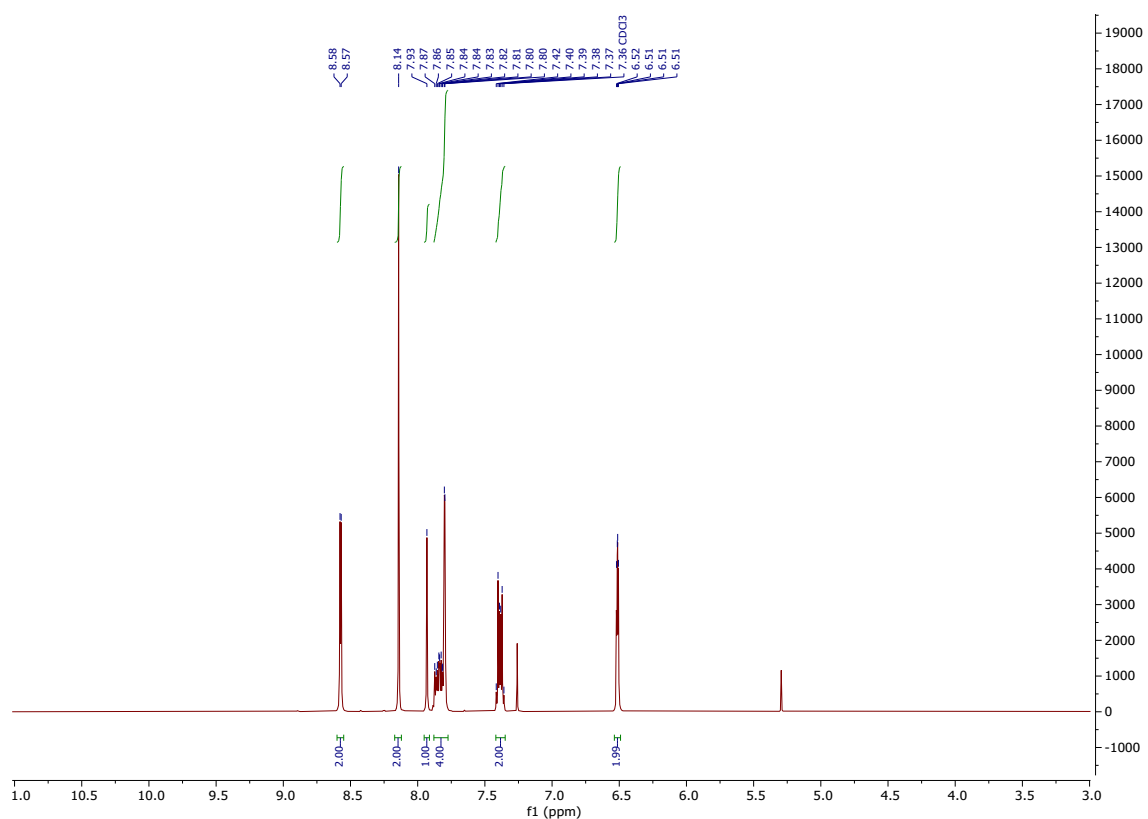


Fig. S14. ^1H NMR (300 MHz, Chloroform-*d*) L^1

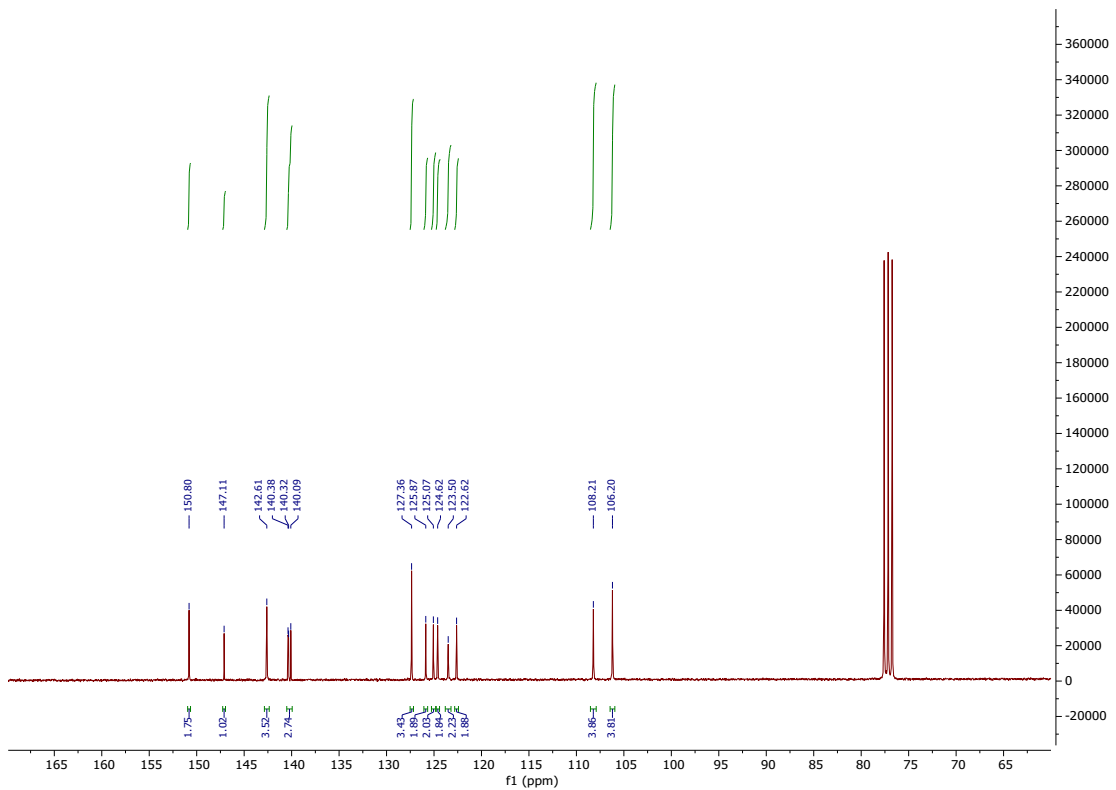


Fig. S15. ^{13}C NMR (126 MHz, Chloroform-*d*) L^1

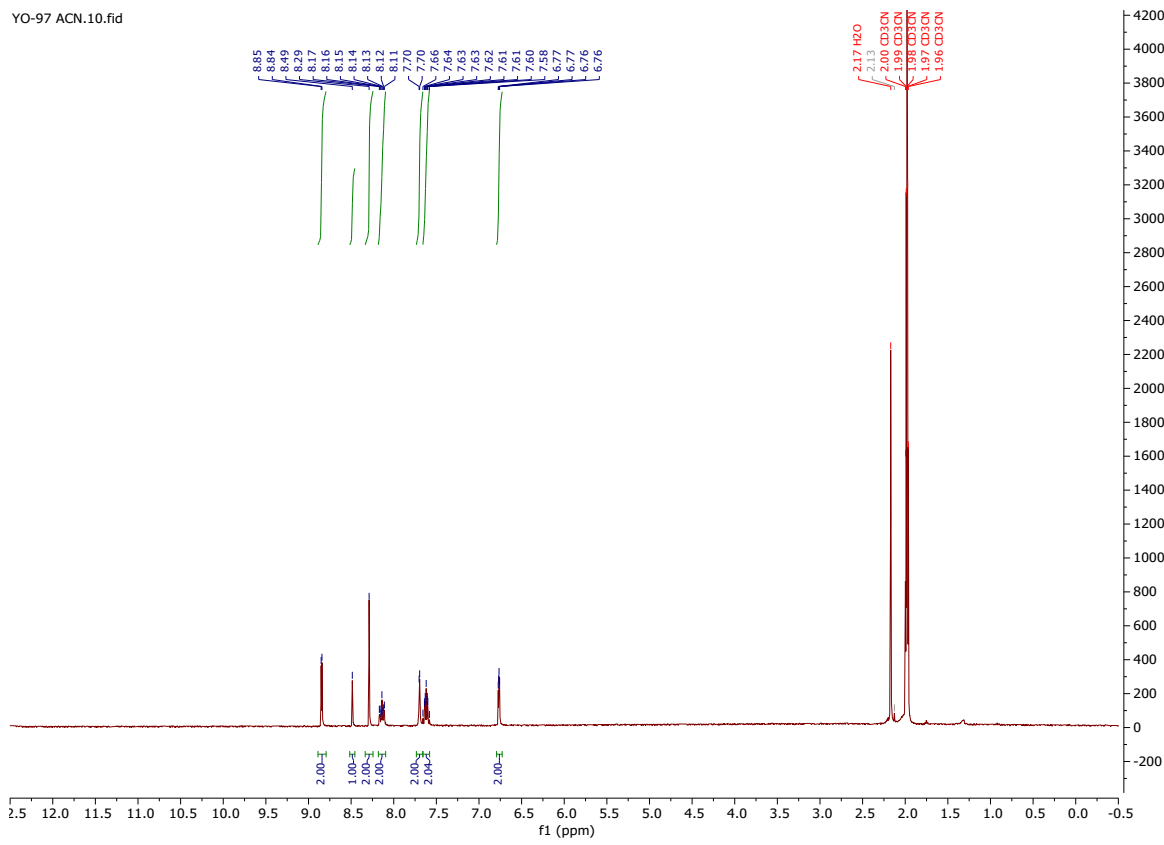


Fig. S16. ^1H NMR (300 MHz, Acetonitrile- d_3) **ZnL¹**

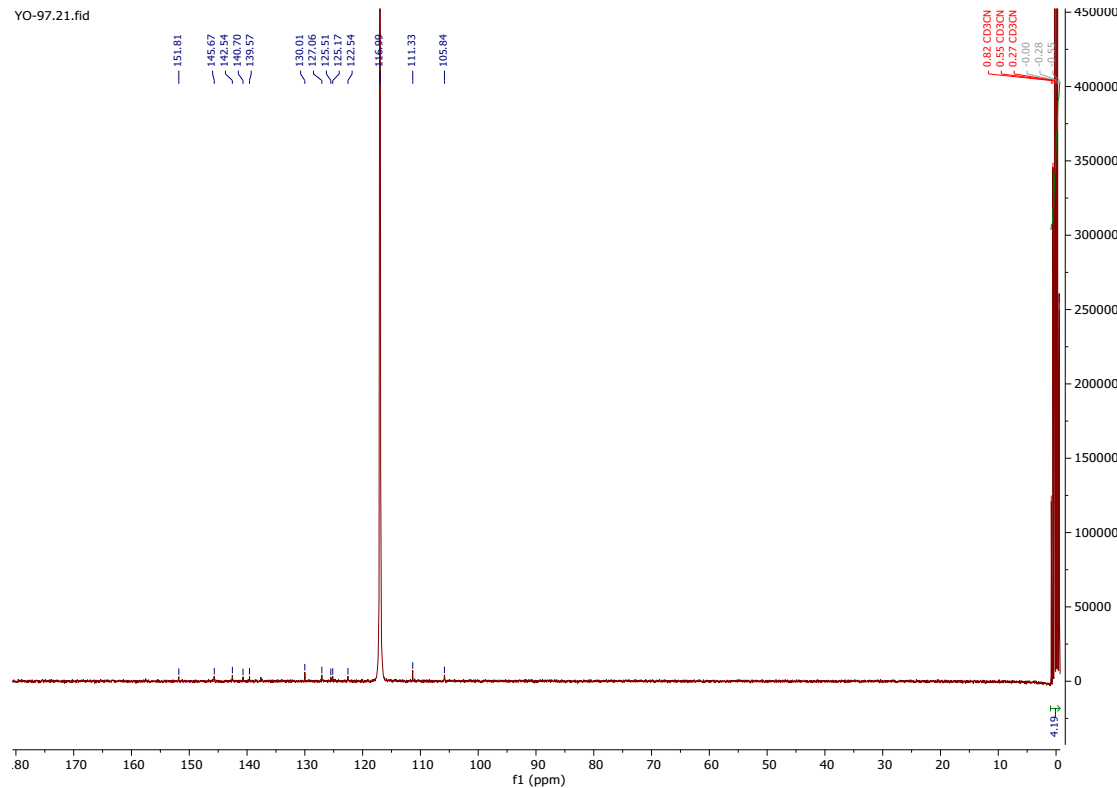


Fig. S17. ^{13}C NMR (126 MHz, Acetonitrile- d_3) **ZnL¹**

YO-62 final.10.fid

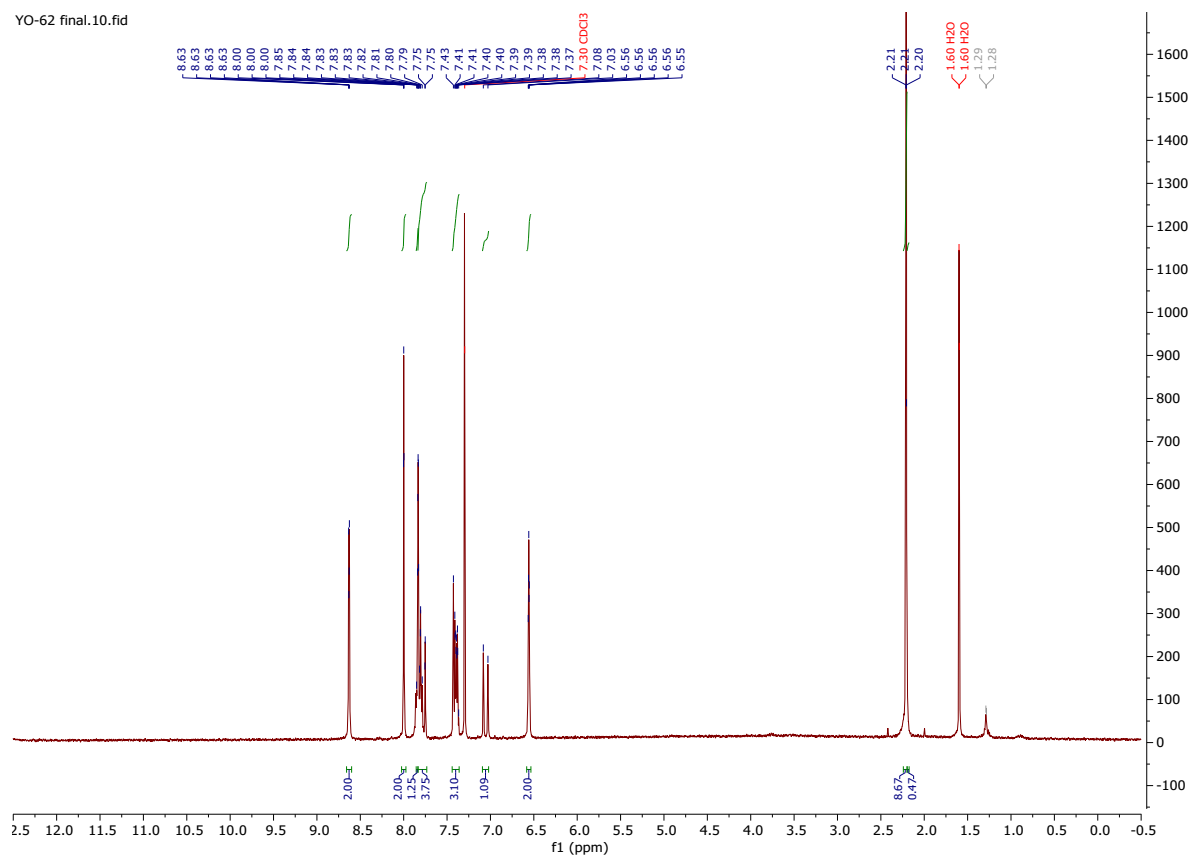


Fig. S18. ^1H NMR (300 MHz, Chloroform- d) L^2

YO-62 final.20.fid

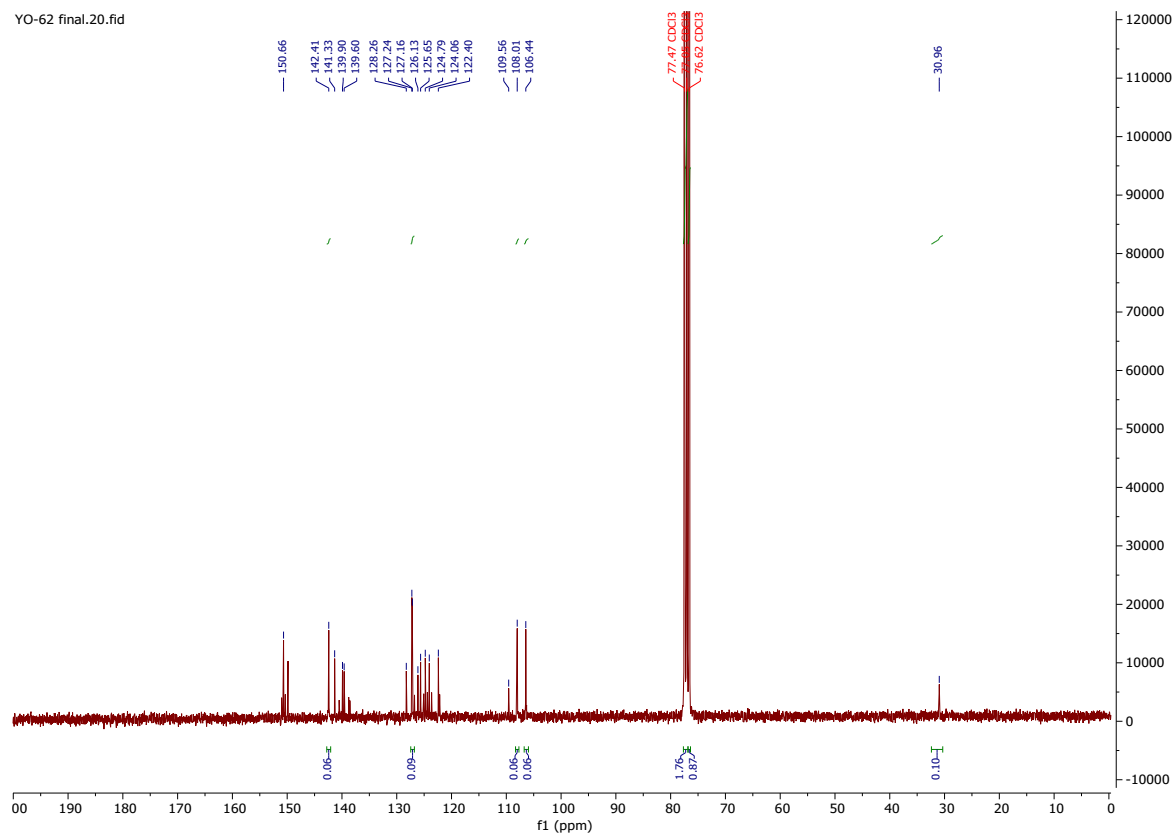


Fig. S19. ^{13}C NMR (126 MHz, Chloroform- d) L^2

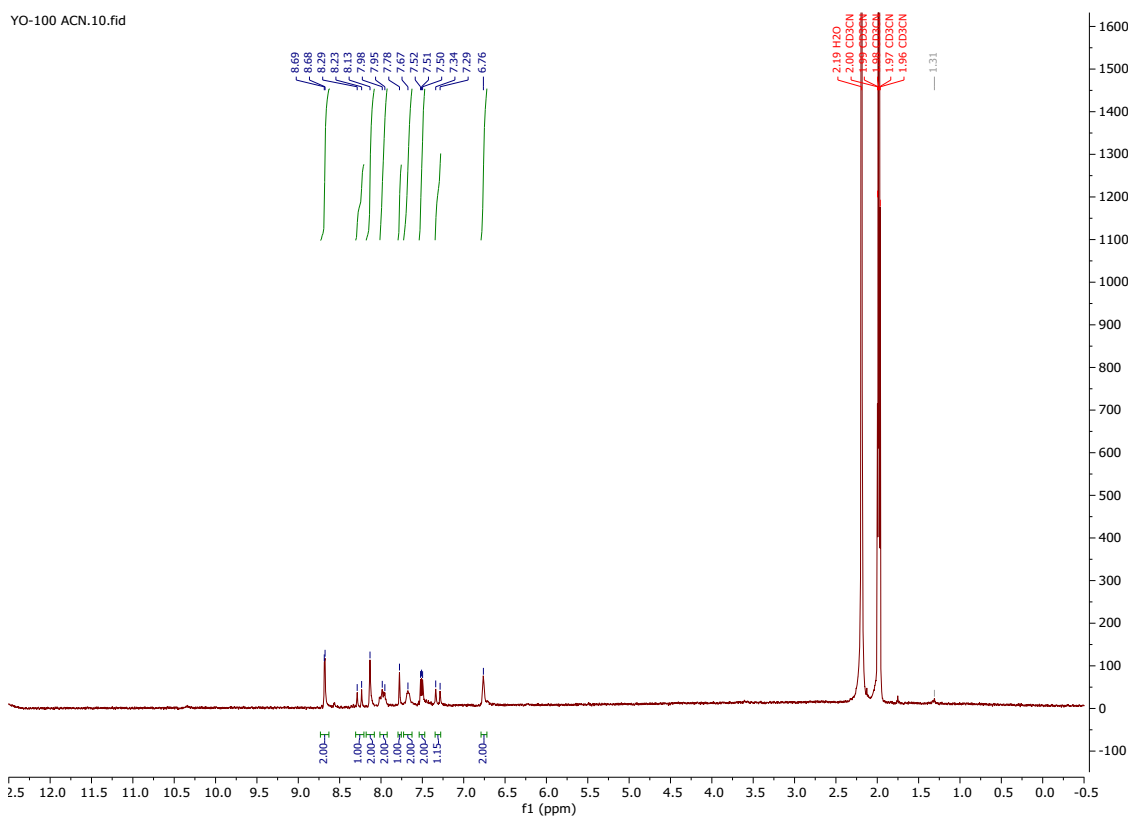


Fig. S20. ^1H NMR (300 MHz, Acetonitrile- d_3) ZnL^2

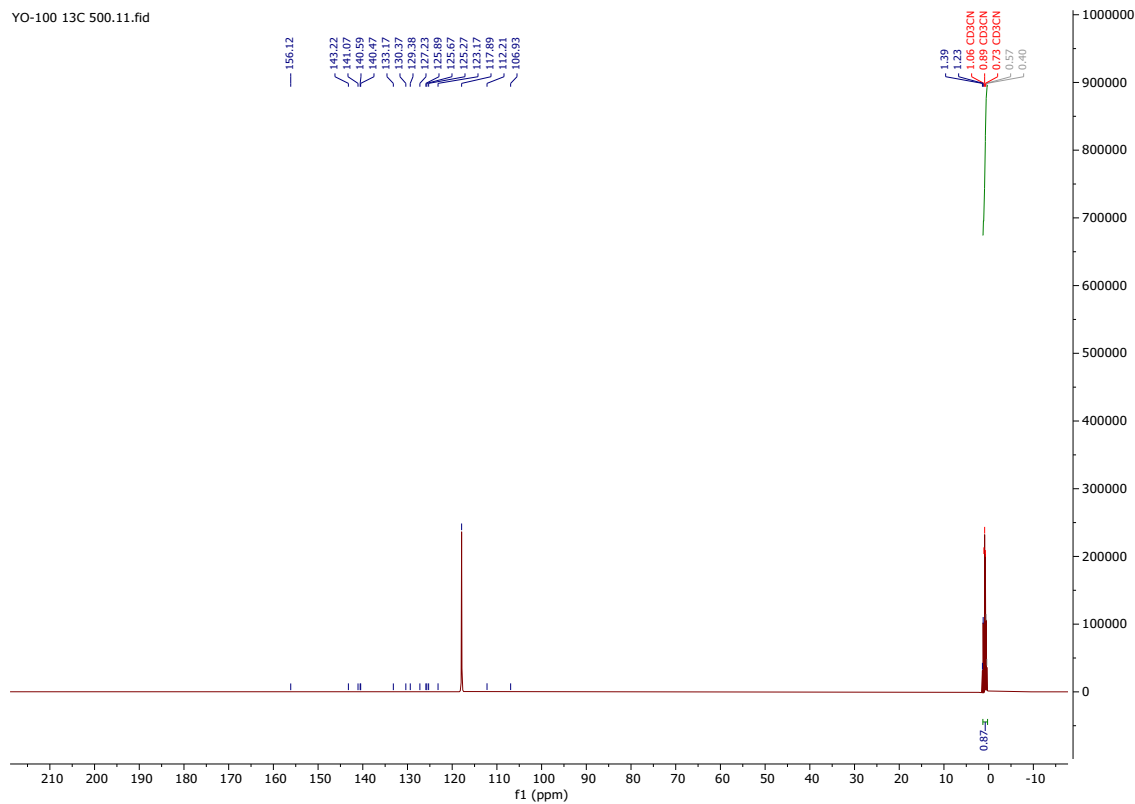


Fig. S21. ^{13}C NMR ((126 MHz, Acetonitrile- d_3) ZnL^2

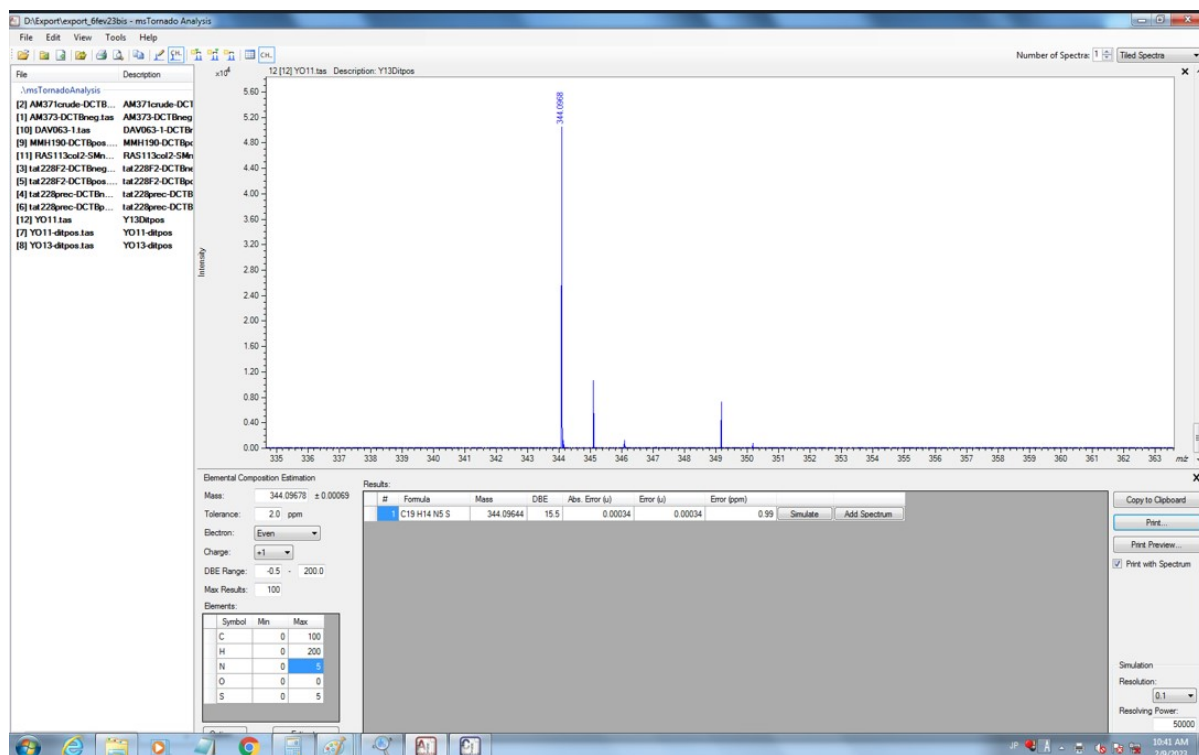


Fig. S22. ESI-MS: L¹

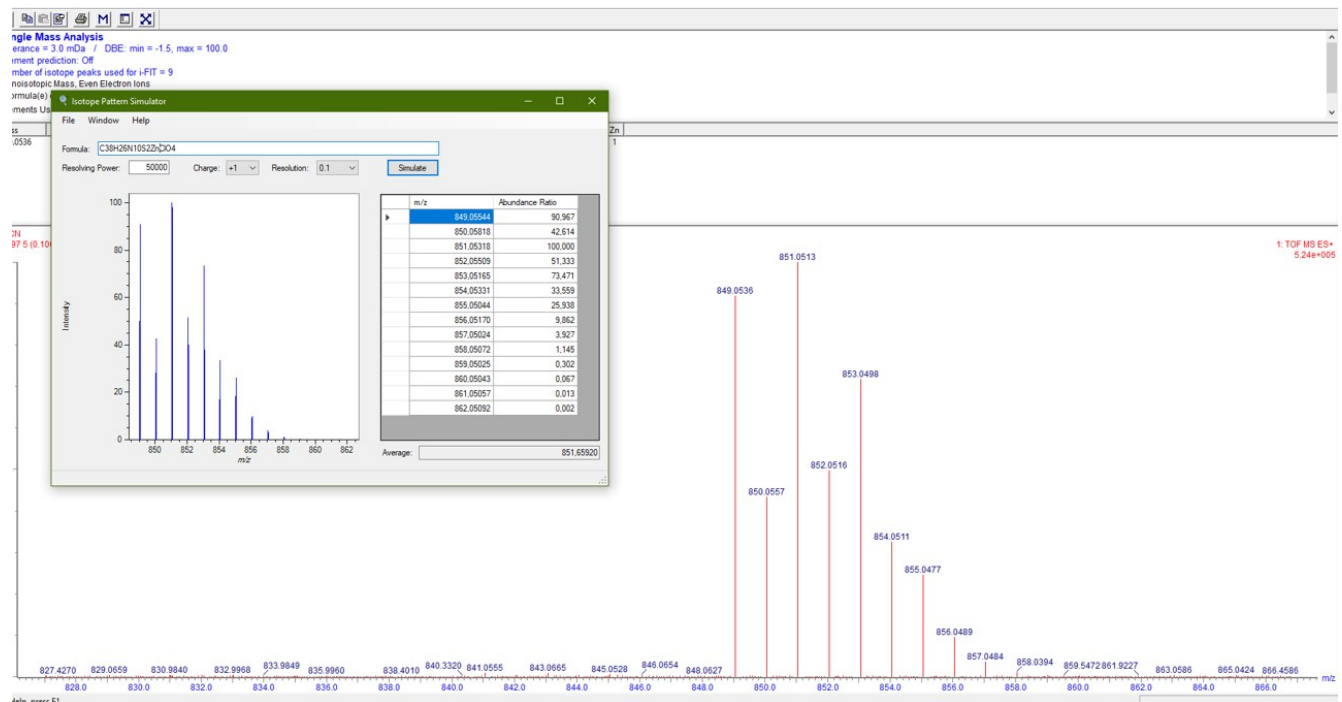


Fig. S23. ESI-MS: ZnL¹

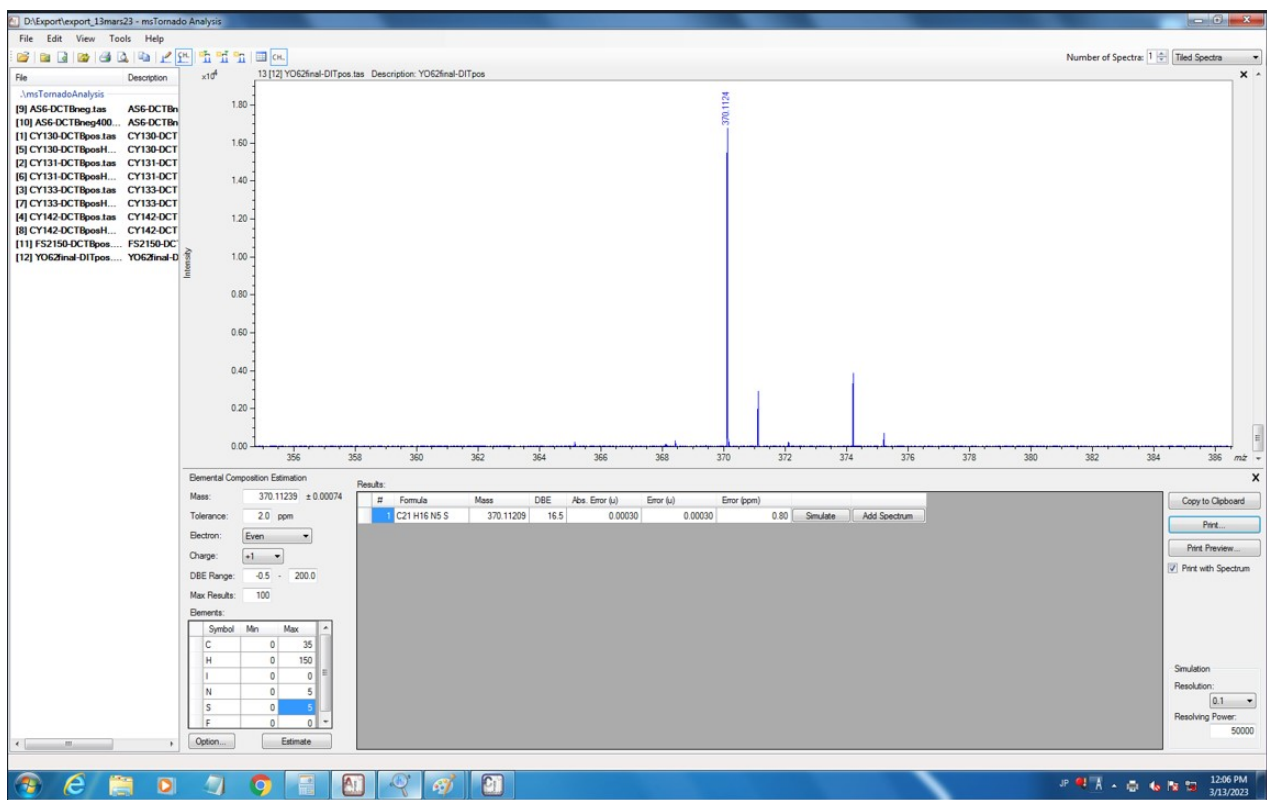


Fig. S24. HR-MS: L²

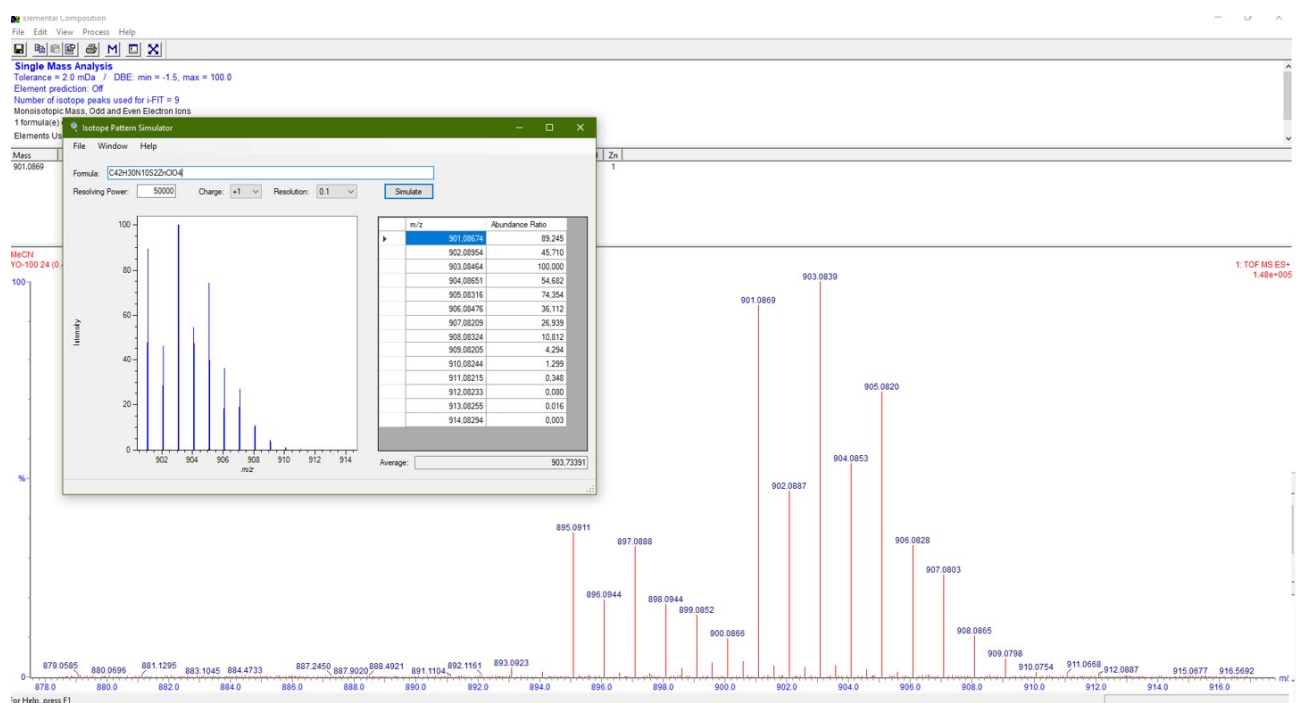


Fig. S25. ESI-MS: ZnL²